

Sea surface roughness modulation by oceanic front: Multi-angle airborne observation during LASER drifter experiment

**N. Rasclé^{1*}, J. Molemaker¹, Louis Marié¹, Frédéric Nougier¹, Björn Lund², Alexis
Mouche¹, Bertrand Chapron¹**

¹Univ. Brest, CNRS, IRD, Ifremer, Laboratoire d'Océanographie Physique et Spatiale (LOPS), IUEM, Brest, France
²Department of Ocean Sciences, Rosenstiel School of Marine and Atmospheric Science, University of Miami, Miami,
Florida, USA

Key Points:

- Sea surface roughness anomaly over an oceanic front is measured during a drifter experiment.
- Multiple passes with an airplane provide measurements at many different azimuth angles.
- The multi-angle roughness anomaly is anisotropic and consistent with anisotropic current gradients.

*Laboratoire d'Océanographie Physique et Spatiale, IFREMER, ZI Pointe du Diable, 29280 Plouzané, France

Corresponding author: Nicolas Rasclé, nicolas.rasclé@ifremer.fr

Abstract

Sea surface roughness contains important geophysical information about the fine scale current gradients at the ocean surface. To better understand this information, we use observations at multiple azimuth view angles. The idea is that the different horizontal current gradient components create different surface roughness anomalies when viewed from different azimuthal directions. We report here results from a dedicated experiment during the LASER (LAGrangian Submesoscale ExpeRiment) drifters deployment. Sun glitter reflections during multiple passes over an oceanic front are used to reconstruct the multi-angle anomaly of surface roughness. Results clearly indicate an anisotropic surface roughness anomaly. In the viewing angle diagram, the zone of contrast inversion is elongated along the wind direction. This multi-angle anomaly is consistent with wave-current interactions over a front with both cross-front convergence and along-front shear with positive vorticity. Such current gradient features are consistent with observed drifters trajectories.

1 Introduction

Surface roughness images often capture spectacular manifestations of fine scale upper ocean dynamics, including internal waves, fronts, filaments and spiraling eddies, at scales between 10 km and down to less than 100 m [e.g. *Fu and Holt*, 1983; *Alpers*, 1985]. Those images are routinely obtained with high-resolution satellite sensors, e.g. from passive optical radiometers viewing areas in and around the sun glitter [e.g. *Scully-Power*, 1986; *Raschle et al.*, 2016] and from active radar instruments like Synthetic Aperture Radars (SARs) [e.g. *Apel et al.*, 1975; *Beal et al.*, 1981; *Kudryavtsev et al.*, 2012a]. In the near future, the multiplication of nano-satellites and possibly drones will provide a huge source of ocean observations at high resolution. The challenge is to develop our ability to extract the geophysical content of those data.

As presently understood, the fine scale features observed on surface roughness images are due to modulations of short (wavelength ~ 1 m) wind waves by horizontal current gradients. Those modulations can be essentially related to three mechanisms. (I) The presence of surfactants, possibly accumulated in zones of surface current convergence, can damp short gravity waves [e.g. *Espedal et al.*, 1998]. (II) The modification of sea surface properties (temperature, current or roughness) can alter the atmospheric boundary layer and thus modify the wind, which in turns modifies short waves [e.g. *Beal et al.*, 1997]. (III) Surface current gradients can directly refract or alter the short scale wave field [e.g. *Phillips*, 1984]. Mechanism (I) due to convergence processes and surfactants [e.g. *McWilliams et al.*, 2009] is likely limited to very low wind speed, except for isolated cases of marine pollution. Mechanism (II) involves modification of the atmospheric boundary layer which seemingly occurs at larger spatial scales than current refraction [*Kudryavtsev et al.*, 2005]. In the present paper, we focus on mechanism (III) as it is likely the principal mechanism explaining surface roughness modifications at fine spatial scales.

To better understand mechanism (III), we propose to use optical observations at multiple azimuth view angles. The idea is that the different components of the horizontal current gradient should create different surface roughness modifications when viewed from different azimuthal directions. In particular, the isotropic divergence of the current has a perfect directional symmetry, and should thus create surface roughness modifications independent on azimuthal view direction, as wind waves propagating in any direction experience similar current gradient. On the contrary anisotropic components of the current gradient like vorticity or strain should create anisotropic surface roughness modifications. This is illustrated in fig. 1. The background (i.e. unperturbed by current) wind-waves are supposed to have a nearly Gaussian slope distribution, with $P_0(z_x, z_y)$ the probability density function (PDF) of eastward z_x and northward z_y slopes. An isotropic current divergence creates an anomalous slope distribution $P = P_0 + P'$ which exhibits a quasi-circular

contrast P'/P compared to the background. On the contrary, an anisotropic current gradient, e.g. a current strain, creates an anisotropic distribution of slopes contrast.

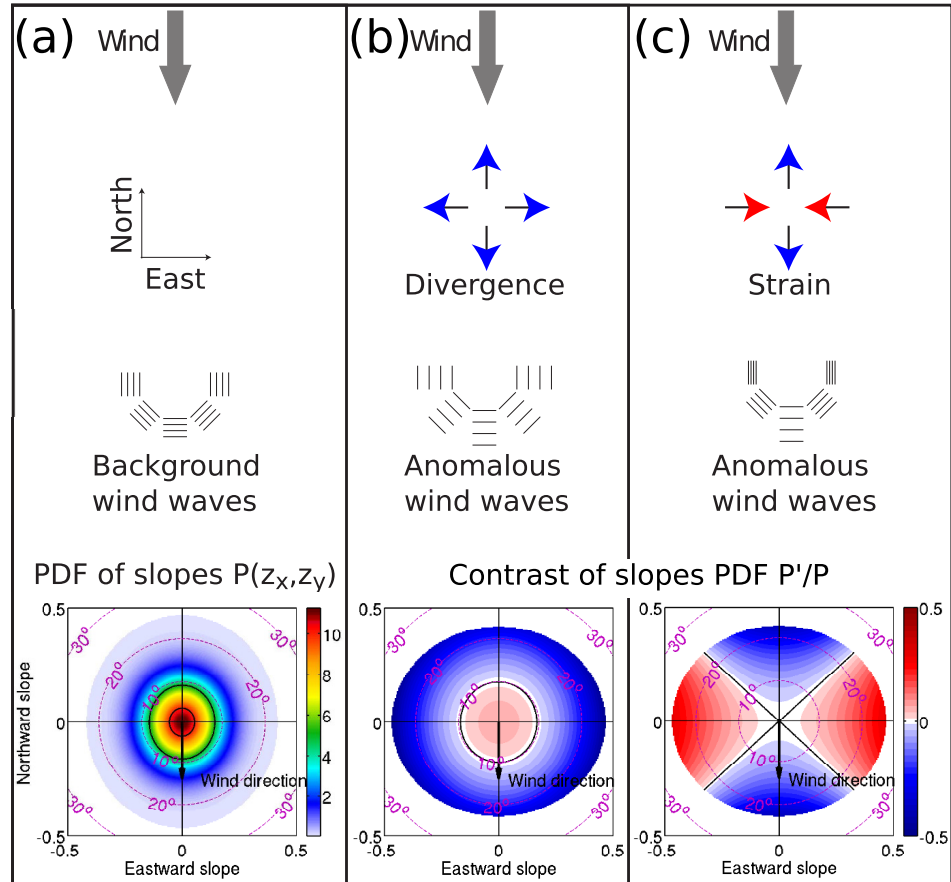


Figure 1. (a) Sketch of the background wind waves and the PDF $P(z_x, z_y)$ of eastward and northward slopes. (b-c) Wind wave in the presence of current divergence or strain, and associated PDF contrast P'/P .

Analysing satellite sun glitter images at multiple azimuth view angles, *Rascle et al.* [2016] documented cases where the slopes PDF anomaly at the Gulf Stream front was anisotropic, namely with more roughness in the upwind direction and less in the cross-wind direction. This was interpreted as evidence of anisotropic current gradients, namely strain in the wind direction. Strain is believed to be after divergence the main component of the current gradient to appear on surface roughness images [*Dulov and Kudryavtsev*, 1990; *Rascle et al.*, 2014].

In the present paper, we further document the link between observations at multiple azimuth view angles and current gradient. We report observations from a dedicated experiment during LASER (LAgrangian Submesoscale ExpeRiment), where a large number of drifters were deployed. Sun glitter reflection was measured from an airplane to reconstruct the slopes PDF anomaly induced by an oceanic front (section 2). Compared to a satellite which can only perform one pass over the front, thus providing a maximum of two azimuths view angles at a given zenith angle [e.g. *Rascle et al.*, 2016], the airplane was used to perform multiple passes, providing the surface roughness anomaly at many different azimuth angles. The surface roughness clearly presents anisotropic anomalies (section 3). This anisotropy cannot be explained by the presence of surfactants nor by an isotropic current convergence. It is consistent with a front with crossfrontal convergence

plus alongfront current shear (section 4). The deployed drifters, although most of them were aligned within the front, provide consistent estimates of the current gradients (section 5).

2 The experiment

2.1 The LASER drifter deployment

The present data were obtained on 11-Feb-2016 during the Lagrangian Submesoscale Experiment (LASER), where a large number ($O(1000)$) of surface drifters were deployed within the Gulf of Mexico (fig. 2a). The wind was blowing from the WSW (255°) about 9 m s^{-1} , as revealed from nearby meteorological buoys (NDBC station 42040). A large number of drifters got caught into an oceanic front with a marked SST jump of about $0.5 - 0.7^\circ\text{C}$ (fig. 2b). An airplane (Partenavia P.68) was used to fly over the front at about 1000 m altitude, acquiring SST using an infrared camera and surface roughness using visible cameras looking at the sun glint.

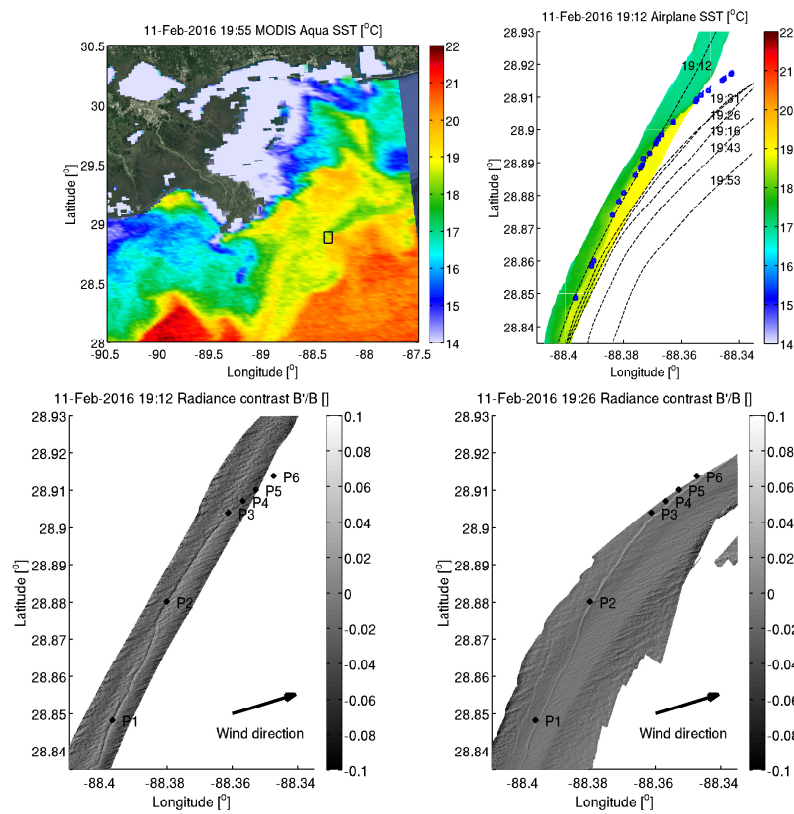


Figure 2. (a) SST from Moderate Resolution Imaging Spectroradiometer (MODIS) [Salomonson *et al.*, 1989] on board *Aqua*. (b,c) SST composite from the first airplane overpass at 19:12 UTC. In (b) the LASER drifters are shown in blue, and the ground tracks of the 6 airplane passes are shown in dashed lines. In (c) the 6 points used for the surface roughness analysis are shown in black. (d) Composite of radiance contrast B'/B at facet angles inside the ellipse of fig. 4f, for the first airplane overpass at 19:12 UTC. (e) Composite for angles outside the ellipse, for the third airplane overpass at 19:26 UTC.

2.2 The visible cameras

The visible light intensity was measured by two panchromatic cameras (JAI BM-500GE) equipped with a 5 mm focal length low distortion lens to ensure a large field of view. The cameras setup is sketched in fig. 3a. The two cameras are arranged symmetrically about the airplane nadir with a pitch of $\pm 35^\circ$ for the forward / aftward cameras. The camera aperture angles are $80^\circ \times 70^\circ$ alongtrack and acrosstrack, respectively, with 2456×2058 pixels in the respective directions. For a flight altitude of 1000 m, this leads to a ground resolution from 0.5 to 6 m. The cameras acquired images at 2 Hz. The images are geolocated using an internal motion unit (Applanix POS AV V610).

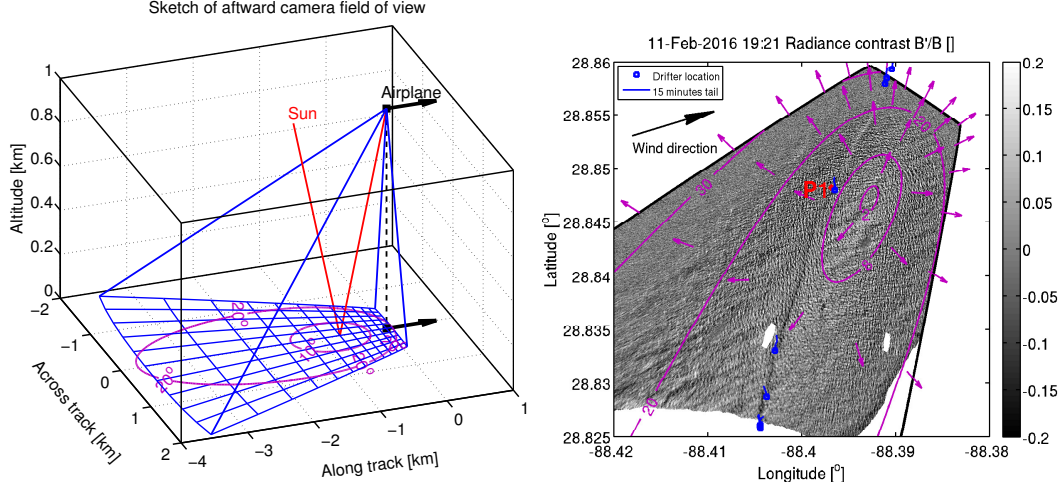


Figure 3. (a) Sketch of the field of view of the aftward camera, for a flight altitude of 1000 m. The varying horizontal resolution is shown with each rectangle representing 200×200 pixels. Here we show the special case of the sun exactly at the rear of the airplane and with a zenith angle of 35° . In such case the specular sun spot is at the center of the camera field of view, and pink contours indicate the zenith angle θ_f of surface facets reflecting the sun. (b) Example of one image of radiance contrast B'/B , at 19:16 UTC, around point P1. Eight drifters (in blue) are caught along the front. Pink contours and arrows indicate respectively the zenith and azimuth angles of the facets reflecting the sun.

2.3 Sun glint and geometry

We consider the surface brightness field in the sun glitter area where the impact of the sky radiance reflected from the surface to the sensor is negligible. Following *Cox and Munk* [1954], the sun glitter radiance, B , generated by specular reflection of the sun light is given as

$$B = \frac{\rho E_s}{4 \cos \theta_c \cos^4 \theta_f} P(z_{xf}, z_{yf}). \quad (1)$$

In this expression, E_s is the sun irradiance, ρ is the Fresnel reflection coefficient, $P(z_x, z_y)$ is the 2D probability density function (PDF) of the eastward (z_x) and northward (z_y) sea surface slopes, and z_{xf} and z_{yf} are the slopes of the surface facet satisfying the conditions of specular reflection of the sun light towards the camera.

The slopes of the specular facet are

$$z_{xf} = -\frac{\sin \theta_s \cos \varphi_s + \sin \theta_c \cos \varphi_c}{\cos \theta_s + \cos \theta_c}, z_{yf} = -\frac{\sin \theta_s \sin \varphi_s + \sin \theta_c \sin \varphi_c}{\cos \theta_s + \cos \theta_c}, \quad (2)$$

where θ_c and θ_s are the camera and sun zenith incidence angles (measured from the vertical), and φ_c and φ_s the camera and sun azimuth angles (measured clockwise from the North). Finally, the zenith and azimuth angles of the specular facet are

$$\theta_f = \arctan \sqrt{z_{xf}^2 + z_{yf}^2}, \quad \varphi_f = \arctan(z_{yf}/z_{xf}). \quad (3)$$

2.4 Radiance contrasts

The observed intensity $B = B_0 + B'$ is separated into a slowly varying background B_0 (mainly due to varying viewing geometry) and a local anomaly B' (due to wave-current interactions) by horizontally filtering with a cut-off scale L . Because of the low flight altitude of 1000 m, L is set to 200 m such that at scales below L the geometry of the observation can be considered constant. Then from (1) one has

$$\frac{B'}{B} = \frac{P'}{P}, \quad (4)$$

i.e. local radiance contrasts are due to slopes PDF contrasts induced by wave-current interactions [Kudryavtsev *et al.*, 2012b]. The idea to extract the geophysical content is to characterize the slopes PDF contrasts P'/P for different viewing geometries, i.e. at different specular facet angles (z_{xf}, z_{yf}) .

3 Observed radiance contrasts over the front

A snapshot of radiance contrast at the front is shown in fig. 3b. We first focus on point P1 within the front¹ (fig. 2 and 3) and compute the radiance contrast compared to neighbouring values outside of the front. Each airplane pass provides a set of observations of P1 at different viewing geometries, more specifically along a line on the slope plane (z_{xf}, z_{yf}) (fig. 4a). As the 6 airplane passes followed slightly different tracks, they provide 6 different lines of observations on the slope plane (z_{xf}, z_{yf}) . Of special interest is the 19:16 pass. It provides in particular two observations at similar zenith angles of $\theta_f \simeq 15^\circ$ but different azimuths φ_f . The radiance contrast at the front is negative for upwind viewing geometry whereas it is positive for crosswind view. Such azimuthal contrast inversion has already been noted from multi-look satellite images by *Rasche et al.* [2016], for the much wider (~ 5 km) front of the Gulf Stream. As satellites only pass once over a region, they do not provide more than two different azimuths at a given zenith view angle. On contrary, the present airplane measurements provide a much more complete view of the surface roughness anomaly, for instance offering up to 10 different azimuth views at a constant zenith angle of 12° .

Additional viewing angles can be obtained if one supposes that the current and surface roughness are uniform in the along-front direction. For instance, the 19:12 track crosses the front North of point P1, around points P3 to P6 (fig.2), which provides different view angles. Fig. 4b cumulates the different passes over the points P1 to P6, giving a more complete description of the radiance contrast at the front. It enables an estimated location of the contrast inversion (fig. 4b, green dotted line), which is clearly elongated along the wind direction. Such multi-angle surface roughness anomalies have not been reported before.

4 Interpretation in terms of current gradient

We hypothesise that wave-current interaction (mechanism III) is responsible for the surface roughness anomaly. To investigate which current gradient could have created such

¹ Within the 40 min of the measurement, the front slightly drifted towards the SE, and the points P1 to P6 are displaced accordingly to remain within the front.

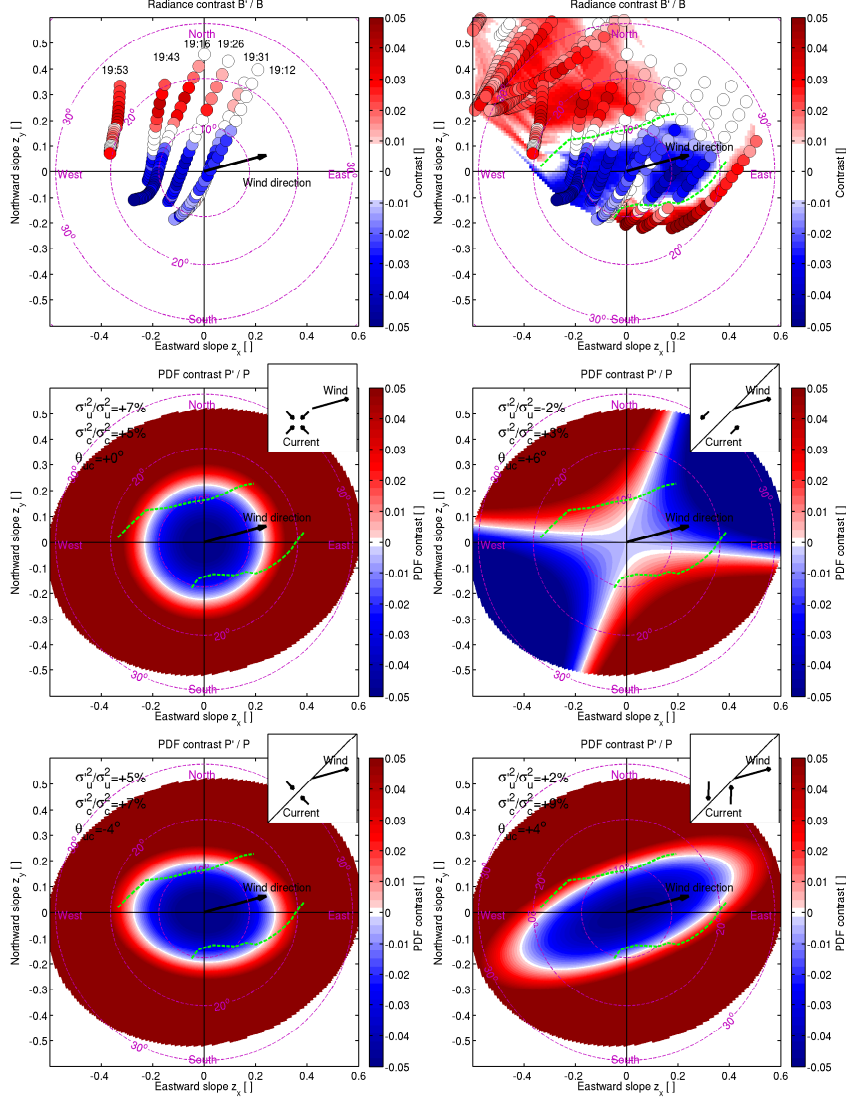


Figure 4. (a-b) Observed radiance contrasts for (a) the 6 passes over point P1, (b) with the additional passes over points P2 to P6. The green dotted line highlights the location of contrast inversion. (c-f) Model PDF contrasts for (c) Isotropic convergence (d) Along front current with shear (e) Across front current with convergence (f) Current as a linear combination $1.2(d) + 0.8(e)$. The wind is set to 9 m s^{-1} from the WSW (255°) and the front orientation is set to SW-NE (45°).

anomaly, we run the model of short waves of *Kudryavtsev et al.* [2005], in its simplified configuration which neglects propagation as described in *Johannessen et al.* [2005]. The wave model calculates the evolution of the spectrum of wave action $N(\mathbf{x}, \mathbf{k})$, where $\mathbf{x} = (x, y)$ is the horizontal position and $\mathbf{k} = (k_x, k_y)$ the wavenumber. Following a relaxation approach [e.g. *Keller and Wright, 1975; Hughes, 1978; Alpers and Hennings, 1984*], the action is written $N(\mathbf{x}, \mathbf{k}) = N_0(\mathbf{k}) + N'(\mathbf{x}, \mathbf{k})$ where N' represents small disturbance with respect to a background value N_0 corresponding to the state undisturbed by currents. The anomaly N' due to local current variations reads

$$N'(\mathbf{x}, \mathbf{k}) = \tau_c \begin{bmatrix} k_x & k_y \end{bmatrix} \begin{bmatrix} \frac{\partial u}{\partial x} & \frac{\partial u}{\partial y} \\ \frac{\partial v}{\partial x} & \frac{\partial v}{\partial y} \end{bmatrix} \begin{bmatrix} \frac{\partial N_0}{\partial k_x} \\ \frac{\partial N_0}{\partial k_y} \end{bmatrix} \quad (5)$$

where $\tau_c(\mathbf{k})$ is a relaxation time scale and (u, v) are the horizontal components of the surface current.

The second moments of the wave spectrum are the upwind m_u , crosswind m_c and cross-correlated m_{uc} mean square slopes (mss), defined by

$$\begin{aligned} mss_u(\mathbf{x}) &= \int \int_{\mathbf{k}} \omega^{-1} k N k_x^2 \mathbf{dk}, \\ mss_c(\mathbf{x}) &= \int \int_{\mathbf{k}} \omega^{-1} k N k_y^2 \mathbf{dk}, \\ mss_{uc}(\mathbf{x}) &= \int \int_{\mathbf{k}} \omega^{-1} k N k_x k_y \mathbf{dk}, \end{aligned} \quad (6)$$

where ω is the intrinsic frequency and without loss of generality we have set here the x -axis in the wind direction.

The PDF of surface slopes is supposed Gaussian and reads [*Longuet-Higgins, 1957*]

$$P(z_x, z_y) = \frac{1}{2\pi\Delta^{1/2}} \exp\left(-\frac{z_x^2 m_c + z_x z_y m_{uc} + z_y^2 m_u}{2\Delta}\right), \quad (7)$$

where $\Delta = m_u m_c - m_{uc}^2$, and where the angle of the principal axis is given by $\tan 2\theta_{uc} = 2m_{uc}/(m_u - m_c)$.

The wind is set to 9 m s⁻¹ from the WSW (255°) and the front orientation is set to SW-NE (45°). We first focus on the sign of the surface roughness anomaly, before considering its magnitude.

4.1 Sign of the current gradient

In the first model run, the current is set to an isotropic convergence (fig. 4c), with a perfect directional symmetry. As illustrated in fig. 1b, waves propagating in any direction experience a compression by the current gradient, increasing the mss in all directions ($m'_u > 0$, $m'_c > 0$). The PDF contrast P'/P is then nearly isotropic, with a contrast inversion occurring at a zenith angle about $\theta_m \simeq \arctan(\sqrt{2m_u}) \simeq 13^\circ$. Such isotropic PDF contrast is similar to that produced by surfactants and reported e.g. by *Cox and Munk* [1954]. The clear anisotropy of our observed radiance contrast points towards anisotropic current gradients.

Following our hypothesis of along-front homogeneity, the current gradients could be a combination of along-front current shear and across-front current divergence. The case of along-front current shear with positive vorticity is shown in fig. 4d. As the wind blows obliquely to the front, it creates a positive strain in the wind direction² which elongates the waves in the wind direction ($m'_u < 0$) and compresses the waves in the crosswind direction ($m'_c > 0$), as illustrated in fig. 1c. The resulting slope PDF is thus separated into four quadrants. The signs of the observed radiance contrast indicates current with positive vorticity, as negative vorticity would produce quadrants of reversed signs.

The case of across-front current convergence is shown in fig. 4e. It is qualitatively similar to the case of isotropic convergence (fig. 4c), except that crosswind waves are slightly more compressed than alongwind waves. As a result the zone of PDF contrast inversion is no longer nearly circular but elongated in the wind direction. The sign of the observed contrast indicates current with positive convergence.

In both cases above, there is a discrepancy between model and observations in terms of the position of the contrast inversion (green dotted line). A correct position of the con-

² To understand this decomposition, see e.g. the fig. 6 in *Raschle et al.* [2016]

trast inversion can be obtained with a combination of positive vorticity plus positive across-front convergence (fig. 4f). The best fit is obtained for a ratio of along-front shear to across-front convergence of the order of 1.5.

Composite images of radiance contrasts B'/B were created for each airplane pass (fig. 2d,e). Observations were separated according to whether the view angle (z_{xf}, z_{yf}) is inside (fig. 2d) or outside (fig. 2e) of the ellipse of contrast inversion shown in fig. 4f. Consistently with our analysis, the front appears with a negative and positive roughness contrast, respectively.

4.2 Amplitude of the current gradient

The amplitude of the surface roughness contrast is related to the wind speed U_{10} , to the amplitude of the current gradient du/dx and to the spatial extent of the current gradient L_u by [see *Kudryavtsev et al.*, 2012b, their eq. 4] $mss' \propto U_{10}^{-1/2} L_u^{-1} du/dx$. A precise estimation requires knowledge of the spatial scale of the surface roughness anomaly, which is limited in our airplane measurements to scales less than $L = 200$ m. Radiance contrasts of the order of 10 to 20% over 50 m are observed at the front. To produce such contrasts at a wind speed of 9 m s^{-1} , the model of *Kudryavtsev et al.* [2005] needs very sharp current variations, of the order of 0.1 m s^{-1} over $L_u = 30$ m (which corresponds to current gradients of $du/dx \approx 45f$, with f the Coriolis parameter) or of the order of 0.3 m s^{-1} over $L_u = 50$ m (corresponding to $du/dx \approx 80f$). Larger values of L_u cannot produce the sharp roughness anomalies observed. A more precise estimation of the current gradient would require roughness observations covering a wider range of spatial scales and will be attempted elsewhere using satellite observations, where the larger sun glitter geometry enables observations at scales up to $L = 20$ km.

5 Current observations and dynamical predictions

Of the order of 300 drifters were deployed in the area during this stage of the LASER experiment. Most of them ended up aligned within the front, which suggests convergence. The trajectory of a few drifters suggests positive vorticity in the vicinity of the front. Also, theoretical studies, numerical simulations [*Roulet and Klein*, 2010] and observations [*Shcherbina et al.*, 2013] suggest that positive vorticity is favoured around oceanic fronts, because intense negative vorticity is subject to instabilities. Those indicate that the current gradient at the front was most likely an across-front convergence and/or an along-front shear with positive vorticity, in qualitative agreement with the slope PDF observed and predicted by the wave model.

Current observations of another filament around the same eddy were obtained 7 hours later using X-band radars on-board R/V Walton Smith REF BJORN?. Those currents were retrieved at 500 m resolution and indicate as expected combinations of across-front convergence and along-front shear with positive vorticity. Current variations about 20 cm s^{-1} are commonly measured between consecutive grid points, leading to gradients about $du/dx \approx 5f$. The present study suggests that those current variations occur at spatial scales an order of magnitude smaller.

6 Conclusion

A dedicated airborne study has been conducted to observe surface roughness anomaly induced by an oceanic front. For the first time, the surface roughness anomaly is documented at many different zenith and azimuth view angles. The anomaly is clearly anisotropic, with an inversion zone elongated along the wind direction. It confirms satellite observations of anisotropic surface roughness [*Raschle et al.*, 2016], and thanks to the airplane ability to perform multiple passes, it provides a quasi complete angular description.

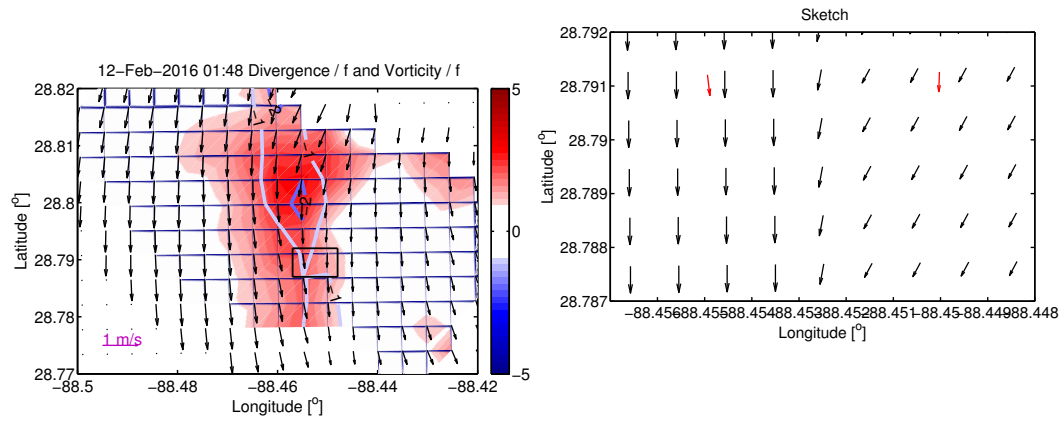


Figure 5. (a) Currents at 500 m resolution observed by X-band radar on Feb. 12th at 01:48 UTC. Contours show divergence and colors show vorticity, both scaled by f . (b) Qualitative sketch zoomed over the box, to show a possible realization of finer scale currents which would match the sharp current gradients estimated from surface roughness observations. The two red arrows are the x-band current observations.

The surface roughness anomaly is related to wave-current interactions. It was expected that, in addition to isotropic current divergence, other anisotropic components of the current, in particular strain in the wind direction [Rascle *et al.*, 2014], should produce surface roughness anomaly. The observed multi-angle anomaly is consistent with anisotropic current gradients, with acrossfront positive convergence plus alongfront shear with a positive vorticity. Those current are consistent with drifter observations and dynamical predictions.

This method of measurement confirms that oceanic fronts might be characterized through their multi-angle surface roughness signature. It advocates for the development of high resolution measurements of surface roughness at multiple azimuth angles to study fine scale ocean dynamics.

Acknowledgments

We acknowledge the financial support of the ANR (French Agence Nationale pour la Recherche) through the REDHOTS project, of the ESA (European Space Agency) through the STSE MESO3D project and through the GlobCurrent project, and of the LabexMer (French Laboratoire d'Excellence) Axe1.

We thank the CARTHE consortium for providing the drifters data.

References

- Alpers, W. (1985), Theory of radar imaging of internal waves, *Nature*, 314(6008), 245–247.
- Alpers, W., and I. Hennings (1984), A theory of the imaging mechanism of underwater bottom topography by real and synthetic aperture radar, *Journal of Geophysical Research: Oceans (1978–2012)*, 89(C6), 10,529–10,546.
- Apel, J. R., H. M. Byrne, J. R. Proni, and R. L. Charnell (1975), Observations of oceanic internal and surface waves from the Earth Resources Technology Satellite, *Journal of Geophysical Research*, 80(6), 865–881.

- Beal, R., V. Kudryavtsev, D. Thompson, S. Grodsky, D. Tilley, V. Dulov, and H. Graber (1997), The influence of the marine atmospheric boundary layer on ERS 1 synthetic aperture radar imagery of the Gulf Stream, *Journal of Geophysical Research: Oceans (1978–2012)*, *102*(C3), 5799–5814.
- Beal, R. C., P. S. DeLeonibus, and I. Katz (1981), *Spaceborne synthetic aperture radar for oceanography*, vol. 7, Johns Hopkins University Press.
- Cox, C., and W. Munk (1954), Measurement of the roughness of the sea surface from photographs of the sun's glitter, *Journal of the optical Society of America*, *44*(11), 838–850.
- Dulov, V., and V. Kudryavtsev (1990), Imagery of the inhomogeneities of currents on the ocean surface state, *Soviet journal of physical oceanography*, *1*(5), 325–336, doi: 10.1007/BF02196830.
- Espedal, H. A., O. M. Johannessen, J. A. Johannessen, E. Dano, D. Lyzenga, and J. Knulst (1998), COASTWATCH'95: ERS 1/2 SAR detection of natural film on the ocean surface, *Journal of Geophysical Research: Oceans (1978–2012)*, *103*(C11), 24,969–24,982.
- Fu, L.-L., and B. Holt (1983), Some examples of detection of oceanic mesoscale eddies by the SEASAT synthetic-aperture radar, *Journal of Geophysical Research: Oceans (1978–2012)*, *88*(C3), 1844–1852.
- Hughes, B. (1978), The effect of internal waves on surface wind waves 2. Theoretical analysis, *Journal of Geophysical Research*, *83*(C1), 455–465.
- Johannessen, J., V. Kudryavtsev, D. Akimov, T. Eldevik, N. Winther, and B. Chapron (2005), On radar imaging of current features: 2. Mesoscale eddy and current front detection, *Journal of Geophysical Research*, *110*, C07,017.
- Keller, W., and J. Wright (1975), Microwave scattering and the straining of wind-generated waves, *Radio Science*, *10*(2), 139–147.
- Kudryavtsev, V., D. Akimov, J. Johannessen, and B. Chapron (2005), On radar imaging of current features: 1. Model and comparison with observations, *Journal of Geophysical Research-Oceans*, *110*(C7), C07,016.
- Kudryavtsev, V., A. Myasoedov, B. Chapron, J. A. Johannessen, and F. Collard (2012a), Imaging mesoscale upper ocean dynamics using synthetic aperture radar and optical data, *Journal of Geophysical Research: Oceans (1978–2012)*, *117*(C4).
- Kudryavtsev, V., A. Myasoedov, B. Chapron, J. A. Johannessen, and F. Collard (2012b), Joint sun-glitter and radar imagery of surface slicks, *Remote Sensing of Environment*, *120*, 123–132.
- Longuet-Higgins, M. S. (1957), The statistical analysis of a random, moving surface, *Philosophical Transactions of the Royal Society of London A: Mathematical, Physical and Engineering Sciences*, *249*(966), 321–387.
- McWilliams, J., F. Colas, and M. Molemaker (2009), Cold filamentary intensification and oceanic surface convergence lines, *Geophysical Research Letters*, *36*(18).
- Phillips, O. M. (1984), On the response of short ocean wave components at a fixed wavenumber to ocean current variations, *Journal of Physical Oceanography*, *14*, 1425–1433.
- Rascle, N., B. Chapron, A. Ponte, F. Ardhuin, and P. Klein (2014), Surface roughness imaging of currents shows divergence and strain in the wind direction, *Journal Of Physical Oceanography*, *44*(8), 2153–2163.
- Rascle, N., F. Nouguier, B. Chapron, A. Mouche, and A. Ponte (2016), Surface roughness changes by fine scale current gradients: Properties at multiple azimuth view angles, *Journal Of Physical Oceanography*, *XX*(X), XXXX–XXXX.
- Roulet, G., and P. Klein (2010), Cyclone-anticyclone asymmetry in geophysical turbulence, *Physical review letters*, *104*(21), 218,501.
- Salomonson, V. V., W. Barnes, P. W. Maymon, H. E. Montgomery, and H. Ostrow (1989), MODIS: Advanced facility instrument for studies of the Earth as a system, *Geoscience and Remote Sensing, IEEE Transactions on*, *27*(2), 145–153.

- Scully-Power, P. (1986), Navy oceanographer shuttle observations, sts 41-g mission report, *Tech. rep.*, DTIC Document.
- Shcherbina, A. Y., E. A. D'Asaro, C. M. Lee, J. M. Klymak, M. J. Molemaker, and J. C. McWilliams (2013), Statistics of vertical vorticity, divergence, and strain in a developed submesoscale turbulence field, *Geophysical Research Letters*, *40*(17), 4706–4711.